Ultrastable and high energy calcium rechargeable batteries enabled by calcium intercalation in a NASICON cathode

Chunhong Chen,[1,3] Fangyi Shi,[1,3] Shishi Zhang,[2] Yaqiong Su,[2] Zheng-Long Xu[1*]

[1] Department of Industrial and Systems Engineering, the Hong Kong Polytechnic University, Hung Hom, Hong Kong, China.

[2] School of Chemistry, Xi'an Key Laboratory of Sustainable Energy Materials Chemistry, State Key Laboratory of Electrical Insulation and Power Equipment, Xi'an Jiaotong University, Xi'an 710049, China.

[3] These authors contributed equally.

[*]Corresponding author: ZL Xu zhenglong.xu@polyu.edu.hk

Abstract

Ca-ion batteries (CIBs) have been considered a promising candidate for the next-generation energy storage technology owing to the abundant calcium element and the low reduction potential of Ca^{2+}/Ca. However, the large size and divalent nature of Ca^{2+} induce significant volume change and sluggish ion mobility in intercalation cathodes, leading to poor reversibly and low energy/power densities for CIBs. Herein, we report a NASICON-typed Na-vacant $Na_1V_2(PO_4)_2F_3$ (N_1PVF_3) with sufficient interstitial spaces as ultra-stable and high-energy Ca ion cathodes. The N_1PVF_3 delivers exceptionally high Ca storage capacities of 110 and 65 mAh g^{-1} at 10 and 500 mA g^{-1}, respectively, and a record-long cyclability of 2000 cycles. More interestingly, by tailoring the fluorine content in N_1PVF_x ($1 \leq x \leq 3$), the high working potential of 3.5 V vs. Ca^{2+}/Ca is achievable. In conjunction with Ca metal anode and a compatible electrolyte, Ca metal batteries with N_1VPF_3 cathodes are constructed, which delivers a high energy density of 342 W h kg^{-1} at the first discharge reaction, representing one of the highest values thus far reported for CIBs. Origins of the uncommonly stable and high-power capabilities for N_1PVF_3 are elucidated as the small volume changes and low cation diffusion barriers among the cathodes.

Keywords: Ca ion battery, cathode material, NASICON structure, full cell.

Introduction

Effective energy storage is considerably imperative to mitigate the energy challenges, such as the limited reserves of fossil fuels and the intermittent solar and wind energy supply.[1-3] Electrochemical energy storage technologies, especially lithium ion batteries (LIBs), have played a central role in putting forward renewable energy utilization. However, the LIBs debated with the controversial lithium raw material supply are approaching their theoretical energy density ceiling, so there is an urgent need to explore new battery chemistries.[4-7] Multivalent (Mg^{2+}, Ca^{2+}, and Al^{3+}) ion batteries are among the top candidates, which utilize more abundant elements.[8-10] Multivalent ion batteries also possess competitive energy densities with monovalent ion (Li^{+}, Na^{+} and K^{+}) batteries by doubling or tripling the number of electron transfer as intercalation of per charge carrier. Among these options, Ca ion battery (CIB) is considered more appealing due to several fundamental merits.[11-14] Ca is the fifth most abundant element (4.86 wt%) in the earth's crust, much less rare than lithium (22 ppm), which would inevitably lower the cost of raw materials for large-scale energy storage applications. The reduction potential of -2.87 V vs. standard hydrogen electrode (SHE) for Ca^{2+}/Ca is more negative than the -2.36 V vs. SHE for Mg^{2+}/Mg and -1.68 V vs. SHE for Al^{3+}/Al, implying higher cell voltages and energy densities. The larger ionic radius of Ca^{2+} (1.14 Å) than Mg^{2+} (0.84 Å) leads to relatively lower polarization strength for Ca^{2+}, suggesting higher Ca^{2+} mobility in electrolyte and cathodes. Together with the better safety (*i.e.*, melting points of 842 ℃ for Ca metal versus 180 ℃ for Li metal) and insensitive dendrite deposition of high capacity Ca metal (1337 mAh g^{-1}), CIBs outstand among the post-LIB technologies.

Recent advances on the development of Ca metal and graphite negative electrodes have brought the rechargeable CIB a step closer to a practically feasible battery system.[15-19] Nevertheless, the progress in discovering desirable cathode materials with high capacity, long-

cycle life and high voltage is laborious. Various material groups have been prepared or hypothesized,[20] such as V_2O_5,[21-22] Ca_xCoO_2 ($0.26 \leq x \leq 0.50$),[23-24] $LiFePO_4$,[25-26] to reversibly store Ca ions as cathodes. Few of them could deliver reasonable cyclic capacities with high working voltages at practically important current densities. The poor electrochemical performance of intercalation cathodes is attributable to the sluggish Ca ion migration kinetics and large volume variations of hosts, stemming from the divalent nature and large size of Ca ions. The divalent Ca^{2+} can induce strong electrostatic interactions with the hosts, posing significant energy barriers for effective Ca^{2+} migration (*e.g.*, ~1.7 eV for Ca diffusion in α-V_2O_5[21, 27], ~2 eV for Ca diffusion in Ca_xMoO_3[28]). Significantly expanded volume changes have been witnessed for Ca ion intercalation cathodes (*e.g.*, up to 30% for spinel $CaMn_2O_4$)[29-31], possibly leading to structural degradation and rapid capacity fading. Therefore, the development of reliable cathodes or strategies to overcome above obstacles is essential to expedite the promotion of CIBs.

Given the similar ionic radii of Ca^{2+} (1.14 Å) and Na^+ (1.16 Å) ions, the proven cathodes in Na ion batteries have recently attracted attention[32-35]. Kim *et al* demonstrated that the $NaV_2(PO_4)_3$ can reversibly cycle 40 times at 3.5 mA g^{-1} in a Ca ion cell using the capacitive activated carbon (AC) as reference electrodes[26]. We also reported an initial Ca ion storage capacity of 78 mAh g^{-1} in the $Na_{0.5}VPO_{4.8}F_{0.7}$ structure[36]. These studies indicate the promise of the polyanionic Na superionic conduction (NASCION) materials for reversible calcium storage. Nevertheless, the moderate calcium storage capacities of below 90 mAh g^{-1}, limited life span of below 500 cycles and few of demonstration for the cathodes in Ca ion full cells justify further innovations to explore the NASICON structures for stable and high energy/power CIBs in practical applications.

In this work, we report a Na-vacant $Na_1V_2(PO_4)_2F_3$ (denoted as N_1VPF_3) as a high capacity, high-voltage and ultra-stable cathode material in CIBs. It is demonstrated that the N_1VPF_3

delivered a high Ca ion storage capacity of approximate 110 mAh g^{-1} with an exceptionally high average voltage of ca. 3.5 V vs. Ca^{2+}/Ca in Ca ion cells and a remarkable cyclability of 81 % capacity retention over 2000 cycles at 250 mA g^{-1}. In addition, the N_1VPF_3 cathode also presents outstanding rate performance with 88 % and 69 % capacity retention as increasing the current density by 50 and 100 folds from 5 mA g^{-1} to 250 and 500 mA g^{-1}, respectively. These values record one of the best performances reported up to date for CIB cathodes. The feasibility of N_1VPF_3 cathode in practical CIBs is confirmed in conjunction with the Ca metal anode and calcium tetrakis(hexafluoroisopropyloxy)borate ($Ca[B(hfip)_4]_2$) ether electrolyte. The N_1VPF_3//Ca metal full cells exhibit an exceptionally high discharge voltage of 3.23 V, a reversible capacity of 106 mAh g^{-1} and hence a record-high energy density of 342 Wh kg^{-1}. The origin of the outstanding performance is also unveiled by intensive experimental and simulation investigations. This study offers a viable approach not only for Ca ion cathode that could eventually lead to high-energy Ca metal batteries, but also in a boarder sense of all multivalent chemistries that faces the similar challenges in searching ultrastable and high-voltage intercalation cathode hosts.

Results and Discussion

Electrochemical performance of N_1VPF_3 in Ca ion cells

The NASICON-typed N_1VPF_3 was synthesized by a typical solid-state reaction method to form $Na_3V_2(PO_4)_2F_3$ (denoted as N_3VPF_3)[37] and followed by electrochemical extraction of two Na ions (see details in Methods and Figure S1 in Supporting Information). The X-ray diffraction (XRD) pattern and Rietveld refinement of the crystal structure show the pure phase N_3VPF_3 with a space group of $P4_2/mnm$ or Amam[38-40], consisting of $V_2O_8F_3$ bioctahedra alternatively bridged by PO_4 tetrahedra (Figures S1b, S2 and S3). After desodiation, XRD patterns indicate that the crystal structure of N_1VPF_3 well maintains a covalent three-dimensional (3D) framework with open cation

diffusion tunnels along [110] and [1$\bar{1}$0] directions. The detailed crystallographic parameters are listed in Tables S1-S2. The morphologies of N_3VPF_3 and N_1VPF_3 were characterized by scanning electron microscopy (SEM) to show nanoparticle structures instead of solid bulks (Figures S1c and S4), which can benefit the charge transfer kinetics by shortening ion diffusion distance during charging/discharging processes.

The Ca-storage performance in the N_1VPF_3 was firstly evaluated in Ca ion half-cells using AC as counter/reference electrodes and the highly stable 0.5 M $Ca(PF_6)_2$ ethylene carbonate/propylene carbonate/ethyl methyl carbonate/dimethyl carbonates (EC/PC/EMC/DMC) as electrolyte at room temperature.[16] The configuration and working process of the Ca ion cells are illustrated in Figure 1a. During discharging, Ca^{2+} ions were intercalated into N_1VPF_3 accompanied by the adsorption of PF_6^- anions into the abundant pores of AC counter electrode. It is noted that AC has been widely used in calcium cathode study to prevent the complexity arising from of the use of Ca metal[41], which is known to be unstable in many aprotic electrolyte systems. Cyclic voltammetry (CV) measurements were conducted to identify the Ca ion intercalation/extraction reactions over a voltage window of -1.0 to 1.5 V vs. AC, which is corresponding to the voltage ranging from 1.75 to 4.25 V vs. Ca^{2+}/Ca base on the voltage calibration in our previous work.[36] A predominant pair of anodic and cathodic peaks at 0.89/0.86 V and two relatively weak redox couples at 0.60/0.36 V and 1.50/1.42 V are clearly observed in Figure 1b, implying a multiple-phase transition during Ca ion (de)intercalation. An extremely low polarization of 31 mV was demonstrated for the predominant redox couple, which is indicative of the rapid electrochemical kinetics of N_1VPF_3 cathode. Moreover, the CV curves of initial several cycles are highly overlapped with negligible discrepancy, suggesting excellent reversibility of the cathode material.

Figure 1c presents the galvanostatic charge/discharge (GCD) voltage profiles of N_1VPF_3. It exhibits an average discharge voltage of 3.5 V vs. Ca^{2+}/Ca and a specific discharge capacity of approximate 110 mAh g^{-1} at 10 mA g^{-1} with a coulombic efficiency (CE) of 95% at the 2nd cycle, corresponding to an intercalation of 0.76 mole Ca^{2+} per formula unit. Similar to the CV profiles, no discernible change was observed for the electrochemical profiles during the first ten cycles, again indicating the excellent reversibility of the N_1VPF_3 cathode. The rate capability of the N_1VPF_3 was evaluated by cycling the Ca ion cells at increasing current densities from 5 to 500 mA g^{-1}, as depicted in Figure 1 d and e. Appreciable discharge capacities of 95, 85, and 65 mAh g^{-1} were recorded at high current densities of 100, 200, and 500 mA g^{-1}, respectively. It manifests that the current density increasing by 50-folds from 10 to 500 mAh g^{-1}, over 50% of the reversible capacity is still retained with trivial increase in over potentials. These results suggest excellent rate performance and superior Ca diffusion kinetics for N_1VPF_3, to be discussed in the kinetics section. When the current density was returned to 10 mA g^{-1}, the initial discharge capacity was recovered and preserved by 96% after another 100 cycles, even after the tough high-rate tests (Figure 1e).

To verify the long-term cyclic stability of the N_1VPF_3 cathode, the Ca ion cells were cycled at a moderate current density of 100 mA g^{-1} for 1100 cycles (Figure S5) and a high rate of 250 mA g^{-1} for 2000 cycles (Figure 1f). It is observed that the N_1VPF_3 delivered a capacity retention of 91 % after 1100 cycles at 100 mA g^{-1}, rendering an extremely low capacity fading rate of 0.008 % per cycle. When cycling at the high rate of 250 mA g^{-1}, the Ca storage capacity was gradually increased to 68 mAh g^{-1} after 400 cycles' activation, and then preserved at 55 mAh g^{-1} at the 2000th cycle, indicating a superb capacity retention of 81% compared to the highest capacity. To estimate the performance of the current N_1VPF_3 cathode among its peers, we summarized the electrochemical performance of the state-of-the-art reported cathodes in CIBs as listed in Table S5 and Figure 1g

[26, 34-36, 41-42]. It clearly illustrates that the N_1VPF_3 outperforms all other cathode materials reported to date with respect to the discharge capacity at a high redox voltage (*i.e.*, 110 mAh g^{-1} at an average working voltage of 3.5 V for N_1VPF_3) and the cyclic stability (*i.e.*, capacity retention of above 81% after over 2000 cycles for N_1VPF_3).

Calcium storage mechanisms in N_1VPF_3 cathode

To obtain deep insights into the calcium storage mechanisms of the N_1VPF_3 cathode possessing remarkable electrochemical performance in calcium electrochemical system, we conducted comprehensive characterizations including *in-situ* XRD, X-ray absorption structure (XAS) and scanning transmission electron microscopy (STEM). First, the structural evolution of the host lattice during Ca (de)intercalation was probed in real time by *in-situ* XRD measurement. The XRD patterns of the N_1VPF_3 cathode were periodically collected when the Ca ion cell was charged and discharged at 10 mA g^{-1} between -1 and 1.5 V vs. AC. The full diffractograms are provided in Figure S6 and the augmented view of the representative XRD peaks is displayed in Figure 2a. During the early stage of Ca^{2+} intercalation, the major peaks at 16.7º, 28.7º, and 33.3º, corresponding to (111), (220), (222) planes of N_1VPF_3 continuously shifted to lower angles while the peak at 16.8º, referring to the (002) plane, gradually moved toward the higher angle. The continuous peak shift suggests a solid-solution reaction region. As following, a new peak at 28º appeared and intensified along with vanish of the peak intensity for the pristine (220) reflection upon further calciation, suggesting a two-phase reaction region (Figure S6). The XRD pattern of fully calciated N_1VPF_3 is consistent with the high-resolution powder XRD result (Figure S2), signifying the reliability of the in-situ characterization. When charging the cell back to 1.5 V, the XRD peaks returned to their original positions, illustrating entire reversibility of the N_1VPF_3 structure during Ca (de)intercalation.

In order to reveal the detailed structural evolution of N_1VPF_3 during calciation/decalciation, Rietveld refinements of the pristine, calciated and decalciated N_1VPF_3 materials are provided in Figure S2 and tabulated in Tables S2-S4. The positions and stoichiometries of Ca and Na in pristine and calciated N_1VPF_3 reveal that 0.7 mol Ca ions occupy the approximate 2 mol Na-vacant interstitial sites in N_1VPF_3 after full calciation. After decalciation, almost all the Ca ions were extracted, leaving the decalciated N_1VPF_3 the comparable crystal structure to the pristine N_1VPF_3 host, indicating excellent reversibility of Ca insertion/extraction in the open framework. The lattice parameters *a* and *c*, corresponding to the basal dimension and the interlayer distance of the N_1VPF_3 crystal structure (Figure 2b), can also be determined by the Rietveld refinement of high-resolution XRD patterns. After calciation, it shows that the lattice parameter *c* (layer stacking direction) slightly contracted by 0.8 %, due to the reduced electrostatic repulsion of O^{2-} layers as screened by the intercalation of positive Ca^{2+} layer in between. On the other hand, the electrochemical reduction of vanadium ions during calciation leads to an expansion in the lattice parameter *a* by 2.1 %. The reverse variation behaviors for lattice parameters *a* and *c* manifest an ultra-small unit volume change of 0.9 % for the N_1VPF_3 cathode during Ca ion intercalation reaction. This value is extremely low considering the large ionic size and the strong electrostatic repulsion between Ca^{2+} and cations in the N_1VPF_3 host. The ultralow volume change can be attributed to two aspects: (i) the NVPF cathode is intrinsically insensitive to volume change owing to its rigid open framework, which has been intensively confirmed in Na-ion batteries,[38-40] and (ii) the divalent Ca^{2+} only needs to occupy half of the interstitial vacancies left by similar sized Na^+ to achieve the same amount of electron transfer, thus involving a smaller volume change in the host (e.g., a volume variation of 2.9 % is reported for Na ion insertion/extraction in N_3VPF_3).[37] We believe

that the small volume change and reversible structure evolution of the N_1VPF_3 framework should be responsible for the outstanding cycling durability in Ca ion cells.

The normalized X-ray absorption near-edge structure (XANES) of N_1VPF_3 at V K-edge with different state of (de)calciation was carried out to evaluate the local structural change and the oxidation/reduction stages of V redox center (Figure 2c). The intensity and energy position of the pre-edge peaks correlating with the valence state of V, suggest that the V^{n+} in pristine N_3PVF_3 was almost the same as that of V^{3+} (V_2O_3), much smaller than that of V^{5+} (V_2O_5). During Ca ion extraction reaction, the edges of absorption spectra shifted apparently toward higher energy region and the intensity of the pre-edge peaks increased clearly for the charged state (marked with arrows), indicating an oxidation of the vanadium ion. When the cathodes were fully discharged in Ca ion cells to -1 V, the spectrum recovers continuously to almost the same pre-edge intensity and profile as the pristine N_3PVF_3, implying that the vanadium redox reaction is fully reversible. The interatomic distance information of the local environment around the transition metal (TM) V atom was further investigated by extended X-ray absorption fine structure (EXAFS) spectra (Figure 2d). The first peak in the Fourier-transformed (FT) EXAFS data is stemming from the scattering of the nearest neighbor oxygen/fluorine (O/F) atoms. Attenuate FT-magnitude and shortened interatomic distance of the first TM-O/F coordination shell are observed at the V K-edge upon Ca deintercalated from the crystal lattice. After discharging to -1 V, both the amplitude and interatomic distances were recovered to the signal for pristine N_3PVF_3, further suggesting entire reversibility of the local structure during Ca ion insertion/extraction reactions.

The intercalation of Ca ions in N_1VPF_3 cathode could be directly confirmed using high-angle annular dark-field scanning transmission-electron microscopy (HAADF-STEM) and the electron energy-loss spectroscopy (EELS). The HAADF image of the calciated N_1VPF_3 viewed along [110]

direction (Figure 2e) shows that the zigzag stacking of VO_4F_2 octahedral and PO_4 tetrahedral forming the pseudo-layered structure with a *d*-space of 5.4 Å (Figure 2f), which resembles its parent structure N_3VPF_3[43-44], indicating the robustness of the polyanion framework. It is noted that the bright spots in Figure 2f are corresponding to heavy vanadium atoms while the light Na and Ca ions are not visible due to the Z-contrast nature of HAADF-STEM image. As an alternative solution, the presence of Ca ions between the VO_4F_2/PO_4 layers can be validated by Ca L-edge EELS profile in Figure 2g. The appreciable peaks of Ca signal indicate the intercalation of Ca ions in the tunnel sites of N_1VPF_3. Above comprehensive characterizations allow us to conclude that Ca ions are reversibly intercalated in and extracted from the interstitial Na vacant sites of N_1VPF_3 associated with vanadium redox reactions in the calcium electrochemical system, which are the origin of the reversible Ca storage capacities.

Calcium intercalation voltage for N_1VPF_3 cathode

High voltage is a critical parameter to achieve high energy CIBs, especially for Ca metal batteries. To understand the outstanding working voltage of 3.5 V vs Ca^{2+}/Ca for N_1VPF_3, a series of $Na_3(VO_{1-x}PO_4)_2F_{1+2x}$ ($0 \leqslant x \leqslant 1$) as parent hosts are prepared to study the correlation between fluorine content and the calcium storage voltage. As shown in Figure 3a, the shape of the charge/discharge profiles for the $Na_1(VO_{1-x}PO_4)_2F_{1+2x}$ (x= 0 and 0.2, denoted as N_1PVF_1, $N_1PVF_{1.4}$) in Ca ion cells are similar to that of N_1VPF_3, where all the calcium storage capacities are located in the range of 80-90 mAh g^{-1} at a current density of 25 mA g^{-1}. The calculated average discharge voltages for N_1PVF_1, $N_1PVF_{1.4}$, and N_1VPF_3 are 3.0, 3.2, and 3.5 V, respectively, clearly presenting a direct relationship between the fluorine content and the average Ca intercalation voltage. Note that average working voltage is calculated by dividing accumulated energy over capacity. This trend cannot be straightforwardly ascribed to the different redox couples of V^{4+}/V^{5+}

and V^{3+}/V^{4+} for N_1VPF_1 and N_1VPF_3, respectively, because the redox potential of V^{4+}/V^{5+} was reported around 0.66 V higher than the V^{3+}/V^{4+} under standard conditions[45]. It is reported that strong ionic F-V bond can enhance the induction of phosphate anion on the electron cloud of each component atom, reducing the energy required for the redox reaction, and thus increasing potentials for fluorine-rich samples.[46-48] Above analyses suggest that the proper control of fluorine content in the vanadium fluorophosphate structure is an effective strategy to regulate the calcium storage voltage. In addition, the plot of average discharging voltage vs. cycle number at 25 mA g^{-1} in Figure 3b shows negligible voltage degradation after 250 cycles, demonstrating the voltage stability of the N_1PVF_3 cathodes cycling in Ca ion cells.

Calcium ion diffusion kinetics in N_1VPF_3

Having verified the stable and high-voltage insertion of Ca ions in N_1VPF_3, we further attempted to unveil the kinetic behaviors of N_1VPF_3 in calcium electrochemical system by conducting CV and galvanostatic intermittent titration technique (GITT) measurements. The CV is measured at different scanning rates from 0.2 to 2 mV s^{-1} between -1.0 and 1.5 V, as shown in Figure 4a. The peak currents increase with the scan rate while the general shape of the CV profiles keeps similar, suggesting the rapid kinetics of the calciation/decalciation processes. The peak currents (I_p) exhibit a linear relation with the square root of scanning rate ($\upsilon^{1/2}$) (Figure 4b), implying a typical diffusion-controlled behavior for Ca-intercalation/extraction reactions in N_1VPF_3. The Ca^{2+} diffusion coefficients (D_{Ca2+}) were calculated to be approximate 3.65×10^{-11} and 8.87×10^{-11} cm^2 s^{-1} for the main cathodic and anodic peaks, respectively, which values are comparable with the GITT measurement in Figure 4c, d and Figure S7. We also compared the diffusion coefficients with peer cathodes as summarized in Table S6. It illustrates that Ca diffusion coefficients in this work are much higher than those of most reported cathodes for CIBs, other multivalent ion

cathodes and even comparable to the cathodes for monovalent LIBs and SIBs. The superior ion diffusion kinetics should be responsible to the high rate capability of N_1VPF_3.

In order to gain more insights into the diffusion behavior of Ca ion in N_1VPF_3, we also conducted density functional theory (DFT) calculations. As illustrated in Figure 4e and f, two representative diffusion paths were defined for Ca^{2+} diffusion in N_1VPF_3 structure: (1) the intra-unit pathway, and (2) the inter-unit pathway, respectively. The activation barrier through the intra-unit path was about 268 meV, and that for inter-unit path was approximate 785 meV. This suggests the inter-unit hopping of Ca ions should be the rate-determining step while intra-unit path provides fast hopping of Ca^{2+}. The calculated activation barrier of 785 meV for Ca^{2+} migration in hosts is remarkably lower than those previously reported for other multivalent ions in cathodes, e.g. 1.12 eV for Al^{3+} in TiS_2,[49] 1.5 eV for Mg^{2+} in VS_4,[50] 0.91 eV for Zn^{2+} in VSe_2.[51] The low energy barriers and the two-dimensional diffusional pathways were conducive to the rapid migration of Ca atoms in N_1VPF_3, supporting the excellent reaction kinetics of Ca^{2+} ion (de)intercalation in the NASICON host cathode.

Ca ion full cells

Finally, to verify the feasibility of N_1VPF_3 in practical application, Ca ion full cells were assembled using the Ca metal anode and the 0.5 M $Ca[B(hfip)_4]_2$ glyme electrolyte,[52] which were cycled at 10 mA g^{-1} between 1.5 and 4.5 V vs. Ca^{2+}/Ca. The N_1VPF_3//Ca metal full cell exhibits a distinct discharge plateau at 3.8 V and an average working voltage of 3.23 V at room temperature as shown in Figure 5a. The reversible calcium storage capacity was determined to be 106 mA h g^{-1}, which is close to the 110 mAh g^{-1} measured in the Ca ion half-cell using AC anode (Figure 1c). As a result, the energy density of the Ca metal battery can be calculated to be 342 Wh kg^{-1} based on the mass of cathode material. This value exceeds the energy densities of the state-of-art Ca ion full

cells to date (e.g., approximate 240 Wh kg^{-1} for V_2O_5//Ca metal in ionic liquid electrolyte),[36, 53] proving the promise of N_1VPF_3 cathode in practical applications. Nevertheless, limited cycle life was still observed for the Ca metal battery (Figure 5b) due to the passivation of Ca metal in the borate ester electrolyte with formation and growth of the CaF_2-rich solid electrolyte interphase. Nevertheless, we demonstrate a successful proof of concept here with outstanding energy density and working voltage using N_1VPF_3 cathode material, which is achieved for the first time in the community.

Conclusion

In summary, NASCION-type N_1VPF_3 is demonstrated as an ultrastable, high-voltage and high-power cathode material for sustainable calcium rechargeable batteries at room temperature. The synergistic contributions of the covalent open 3D framework with large tunnel sites and substantial Na interstitial vacancies offers efficient diffusion pathways and Ca ion accommodation places, leading to high Ca^{2+} mobility with suppressed volume change and high Ca storage capacities, respectively. Meanwhile, the high working voltage is particularly determined by the effect of fluorine-rich phase to modulate the redox potential of V^{3+}/V^{4+} couples. On basis of above fundamental merits of the NASICON structure toward Ca ion storage, the N_1VPF_3 delivers attractive electrochemical performance in Ca ion cells with an extraordinarily high average voltage of 3.5 V vs. Ca^{2+}/Ca, a specific capacity of 110 mAh g^{-1} and an extremely long lifetime exceeding 2000 cycles, which rivals with the state-of-art cathode materials reported so far for CIBs. When coupled with the Ca metal anode, the new Ca ion full cells exhibit an outstanding energy density and one of the highest cell voltages. It is expected that findings in this work would set a milestone towards the development of CIBs cathode system and provide a promising inspiration for studying the cathodes in other multivalent-ion batteries.

Reference

[1] B. Dunn, H. Kamath, J.-M. Tarascon, *Science* **2011**, *334*, 928.
[2] F. Wu, J. Maier, Y. Yu, *Chem. Soc. Rev.* **2020**, *49*, 1569.
[3] D. Castelvecchi, E. Stoye, *Nature* **2019**, *574*, 308.
[4] M. Li, J. Lu, X. Ji, Y. Li, Y. Shao, Z. Chen, C. Zhong, K. Amine, *Nat. Rev. Mater.* **2020**, *5*, 276.
[5] F. Duffner, N. Kronemeyer, J. Tübke, J. Leker, M. Winter, R. Schmuch, *Nat. Energy* **2021**, *6*, 123.
[6] J. W. Choi, D. Aurbach, *Nat. Rev. Mater.* **2016**, *1*, 16013.
[7] F. Shi, C. Chen, Z.-L. Xu, *Adv. Fiber Mater.* **2021**, *3*, 275.
[8] Y. Liang, H. Dong, D. Aurbach, Y. Yao, *Nat. Energy* **2020**, *5*, 646.
[9] J. Muldoon, C. B. Bucur, T. Gregory, *Chem. Rev.* **2014**, *114*, 11683.
[10] S. Hou, X. Ji, K. Gaskell, P.-f. Wang, L. Wang, J. Xu, R. Sun, O. Borodin, C. Wang, *Science* **2021**, *374*, 172.
[11] C. Chen, F. Shi, Z.-L. Xu, *J. Mater. Chem. A* **2021**, *9*, 11908.
[12] M. E. Arroyo-de Dompablo, A. Ponrouch, P. Johansson, M. R. Palacín, *Chem. Rev.* **2020**, *120*, 6331.
[13] R. J. Gummow, G. Vamvounis, M. B. Kannan, Y. He, *Adv. Mater.* **2018**, *30*, 1801702.
[14] I. D. Hosein, *ACS Energy Lett.* **2021**, *6*, 1560.
[15] S. J. Richard Prabakar, A. B. Ikhe, W. B. Park, K.-C. Chung, H. Park, K.-J. Kim, D. Ahn, J. S. Kwak, K.-S. Sohn, M. Pyo, *Adv. Sci.* **2019**, *6*, 1902129.
[16] M. Wang, C. Jiang, S. Zhang, X. Song, Y. Tang, H.-M. Cheng, *Nat. Chem.* **2018**, *10*, 667.
[17] J. Park, Z.-L. Xu, G. Yoon, S. K. Park, J. Wang, H. Hyun, H. Park, J. Lim, Y.-J. Ko, Y. S. Yun, K. Kang, *Adv. Mater.* **2020**, *32*, 1904411.
[18] A. Ponrouch, C. Frontera, F. Bardé, M. R. Palacín, *Nat. Mater.* **2016**, *15*, 169.
[19] A. Shyamsunder, L. E. Blanc, A. Assoud, L. F. Nazar, *ACS Energy Lett.* **2019**, *4*, 2271.
[20] A. Torres, J. L. Casals, M. E. Arroyo-de Dompablo, *Chem. Mater.* **2021**, *33*, 2488.
[21] G. S. Gautam, P. Canepa, R. Malik, M. Liu, K. Persson, G. Ceder, *Chem. Commun.* **2015**, *51*, 13619.
[22] R. Verrelli, A. P. Black, C. Pattanathummasid, D. S. Tchitchekova, A. Ponrouch, J. Oró-Solé, C. Frontera, F. Bardé, P. Rozier, M. R. Palacín, *J. Power Sources* **2018**, *407*, 162.
[23] B. L. Cushing, J. B. Wiley, *J. Solid State Chem.* **1998**, *141*, 385.
[24] M. Cabello, F. Nacimiento, J. R. González, G. Ortiz, R. Alcántara, P. Lavela, C. Pérez-Vicente, J. L. Tirado, *Electrochem. Commun.* **2016**, *67*, 59.
[25] K. V. Nielson, J. Luo, T. L. Liu, *Batter. Supercaps* **2020**, *3*, 766.
[26] S. Kim, L. Yin, M. H. Lee, P. Parajuli, L. Blanc, T. T. Fister, H. Park, B. J. Kwon, B. J. Ingram, P. Zapol, R. F. Klie, K. Kang, L. F. Nazar, S. H. Lapidus, J. T. Vaughey, *ACS Energy Lett.* **2020**, *5*, 3203.
[27] A. Parija, D. Prendergast, S. Banerjee, *Acs Appl. Mater. Interfaces* **2017**, *9*, 23756.
[28] M. Baldoni, L. Craco, G. Seifert, S. Leoni, *J. Mater. Chem. A* **2013**, *1*, 1778.
[29] M. Liu, Z. Rong, R. Malik, P. Canepa, A. Jain, G. Ceder, K. A. Persson, *Energ. Environ. Sci.* **2015**, *8*, 964.
[30] M. E. Arroyo-de Dompablo, C. Krich, J. Nava-Avendaño, M. R. Palacín, F. Bardé, *Phys. Chem. Chem. Phys.* **2016**, *18*, 19966.
[31] A. Torres, F. Bardé, M. E. Arroyo-de Dompablo, *Solid State Ionics* **2019**, *340*, 115004.

[32] T. N. Vo, H. Kim, J. Hur, W. Choi, I. T. Kim, *J. Mater. Chem. A* **2018**, *6*, 22645.
[33] A. L. Lipson, B. Pan, S. H. Lapidus, C. Liao, J. T. Vaughey, B. J. Ingram, *Chem. Mater.* **2015**, *27*, 8442.
[34] B. Jeon, J. W. Heo, J. Hyoung, H. H. Kwak, D. M. Lee, S.-T. Hong, *Chem. Mater.* **2020**, *32*, 8772.
[35] J. Wang, S. Tan, F. Xiong, R. Yu, P. Wu, L. Cui, Q. An, *Chem. Commun.* **2020**, *56*, 3805.
[36] Z.-L. Xu, J. Park, J. Wang, H. Moon, G. Yoon, J. Lim, Y.-J. Ko, S.-P. Cho, S.-Y. Lee, K. Kang, *Nat. Commun.* **2021**, *12*, 3369.
[37] Y.-U. Park, D.-H. Seo, H. Kim, J. Kim, S. Lee, B. Kim, K. Kang, *Adv. Funct. Mater.* **2014**, *24*, 4603.
[38] M. Bianchini, N. Brisset, F. Fauth, F. Weill, E. Elkaim, E. Suard, C. Masquelier, L. Croguennec, *Chem. Mater.* **2014**, *26*, 4238.
[39] C. Zhu, C. Wu, C.-C. Chen, P. Kopold, P. A. van Aken, J. Maier, Y. Yu, *Chem. Mater.* **2017**, *29*, 5207.
[40] B. Zhang, R. Dugas, G. Rousse, P. Rozier, A. M. Abakumov, J.-M. Tarascon, *Nat. Commun.* **2016**, *7*, 10308.
[41] X. Xu, M. Duan, Y. Yue, Q. Li, X. Zhang, L. Wu, P. Wu, B. Song, L. Mai, *ACS Energy Lett.* **2019**, *4*, 1328.
[42] W. Ren, F. Xiong, Y. Fan, Y. Xiong, Z. Jian, *Acs Appl. Mater. Interfaces* **2020**, *12*, 10471.
[43] L. Li, Y. Xu, X. Sun, R. Chang, Y. Zhang, X. Zhang, J. Li, *Adv. Energy Mater.* **2018**, *8*, 1801064.
[44] Y. Li, X. Liang, G. Chen, W. Zhong, Q. Deng, F. Zheng, C. Yang, M. Liu, J. Hu, *Chem. Eng. J.* **2020**, *387*, 123952.
[45] Y.-U. Park, D.-H. Seo, H.-S. Kwon, B. Kim, J. Kim, H. Kim, I. Kim, H.-I. Yoo, K. Kang, *J. Am. Chem. Soc.* **2013**, *135*, 13870.
[46] L. Deng, F.-D. Yu, Y. Xia, Y.-S. Jiang, X.-L. Sui, L. Zhao, X.-H. Meng, L.-F. Que, Z.-B. Wang, *Nano Energy* **2021**, *82*, 105659.
[47] N. Recham, J. N. Chotard, J. C. Jumas, L. Laffont, M. Armand, J. M. Tarascon, *Chem. Mater.* **2010**, *22*, 1142.
[48] W. Song, Z. Wu, J. Chen, Q. Lan, Y. Zhu, Y. Yang, C. Pan, H. Hou, M. Jing, X. Ji, *Electrochim. Acta* **2014**, *146*, 142.
[49] V. V. Kulish, D. Koch, S. Manzhos, *Phys. Chem. Chem. Phys.* **2017**, *19*, 6076.
[50] Z. Li, B. P. Vinayan, P. Jankowski, C. Njel, A. Roy, T. Vegge, J. Maibach, J. M. G. Lastra, M. Fichtner, Z. Zhao-Karger, *Angew. Chem. Int. Ed.* **2020**, *59*, 11483.
[51] Z. Wu, C. Lu, Y. Wang, L. Zhang, L. Jiang, W. Tian, C. Cai, Q. Gu, Z. Sun, L. Hu, *Small* **2020**, *16*, 2000698.
[52] Z. Li, O. Fuhr, M. Fichtner, Z. Zhao-Karger, *Energ. Environ. Sci.* **2019**, *12*, 3496.
[53] X. Gao, X. Liu, A. Mariani, G. A. Elia, M. Lechner, C. Streb, S. Passerini, *Energ. Environ. Sci.* **2020**, *13*, 2559.

Acknowledgements

The work described in this paper was fully supported by a grant from the Research Grants Council of the Hong Kong Special Administrative Region, China (Project No. PolyU25216121), the National Natural Science Foundation of China-Youth (Project No. 52102310), the Research

Committee of the Hong Kong Polytechnic University under project codes of BE3M and YWB1. We are grateful for Hao Zhang from Soochow University and Jian Wang from the Hong Kong Polytechnic University aiding in the synchrotron X-ray absorption spectroscopy measurement and analysis.

Author contributions

Z.L.X and C.H.C conceived the idea. C.H.C conducted the experiment and analyzed the data. F.Y.S. assisted on the experiment. S.S.Z and Y.Q.S performed the DFT calculation. Z.L.X. revised the manuscript prepared by C.H.C. All authors commented on the manuscript.

Competing interests

The authors declare no competing interest.

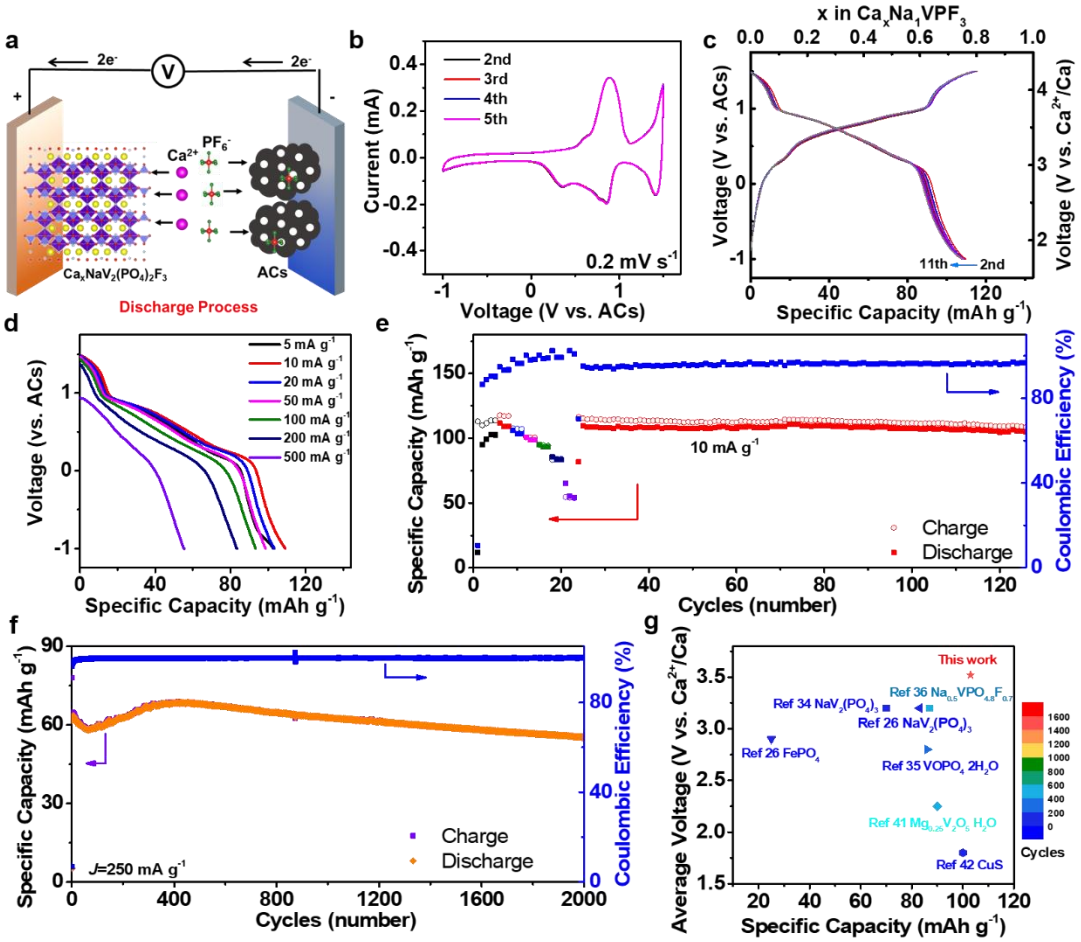

Figure 1. Electrochemical properties of N_1VPF_3 in Ca ion cells. (a) Schematic of the configuration for the half cell, which consists of $Ca_xN_1PVF_3$ cathode, AC anode, and 0.25 M $Ca(PF_6)_2$ EC/PC/DMC/EMC (2:2:3:3 v/v/v/v) electrolyte. (b) CV curves of the N_1VPF_3 electrode at a scan rate of 0.2 mV s^{-1}. (c) Galvanostatic charge and discharge curves of N_1VPF_3 cycled at a current density of 10 mA g^{-1} in the voltage range of -1 to 1.5 V vs. AC. (d) Discharge profiles and (e) the rate capacities of N_1VPF_3 at various rates from 5 mA g^{-1} to 500 mA g^{-1}. (f) Cyclic capacities and coulombic efficiencies of N_1VPF_3 at 250 mA g^{-1} for 2000 cycles. (g) Comparison of the current N_1VPF_3 cathode with previously reported calcium cathodes in terms of specific capacity, average discharge voltage, and cycle number.

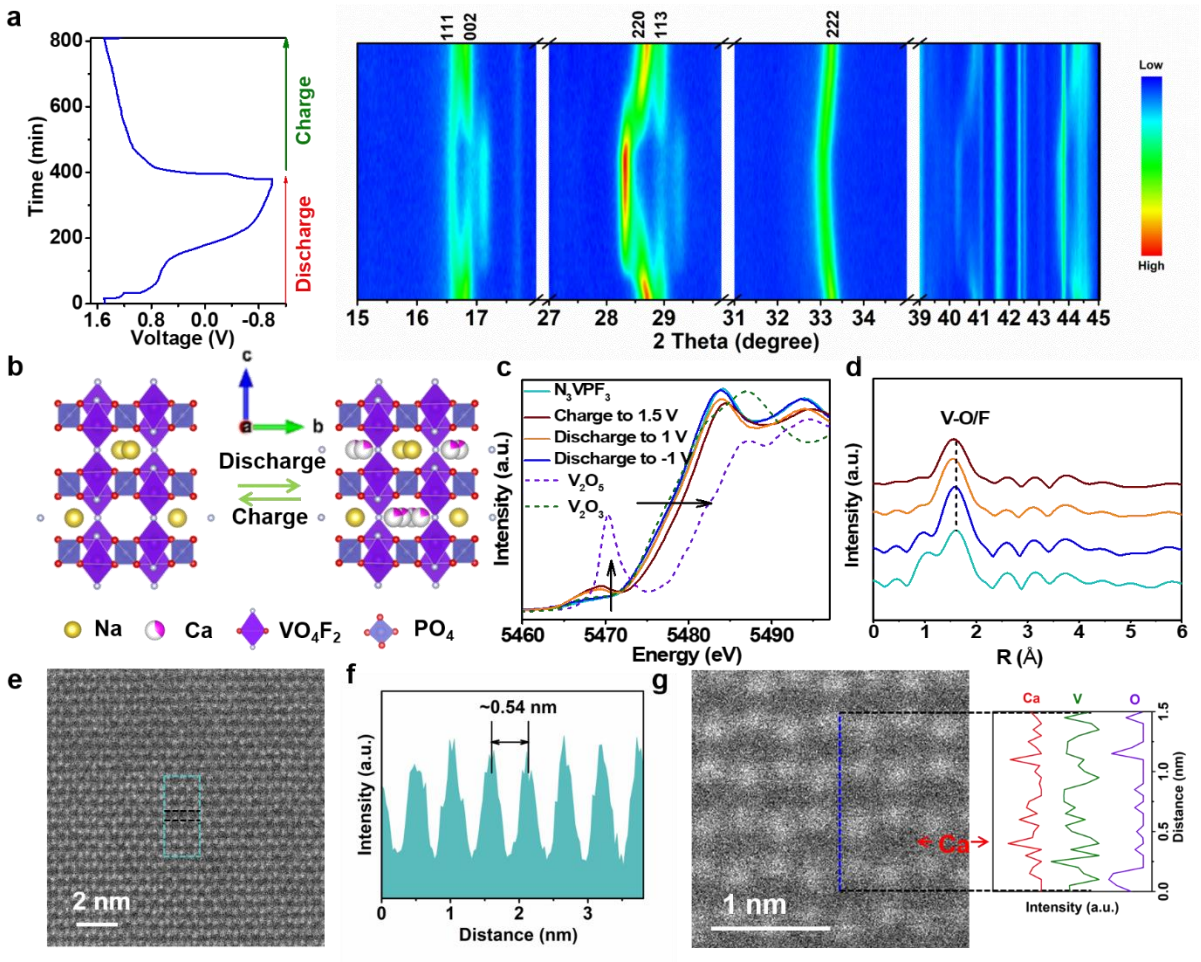

Figure 2. Structural evolution of N_1VPF_3 during the (de)calciation process. (a) The augmented in-situ XRD intensity map for one cycle of the N_1VPF_3 cathode. (b) Schematic illustration of the Ca intercalation/extraction processes in N_1VPF_3. (c) V K-edge XANES and (d) the FT-EXAFS spectra of N_1VPF_3 at different states of charge/discharge. (e) HAADF-STEM image of fully calciated N_1VPF_3. (f) Intensity profiles obtained in marked area in (e). (g) The content distribution of O, V, and Ca EELS signal (right) along the blue line scan in the atomic scale STEM image (left).

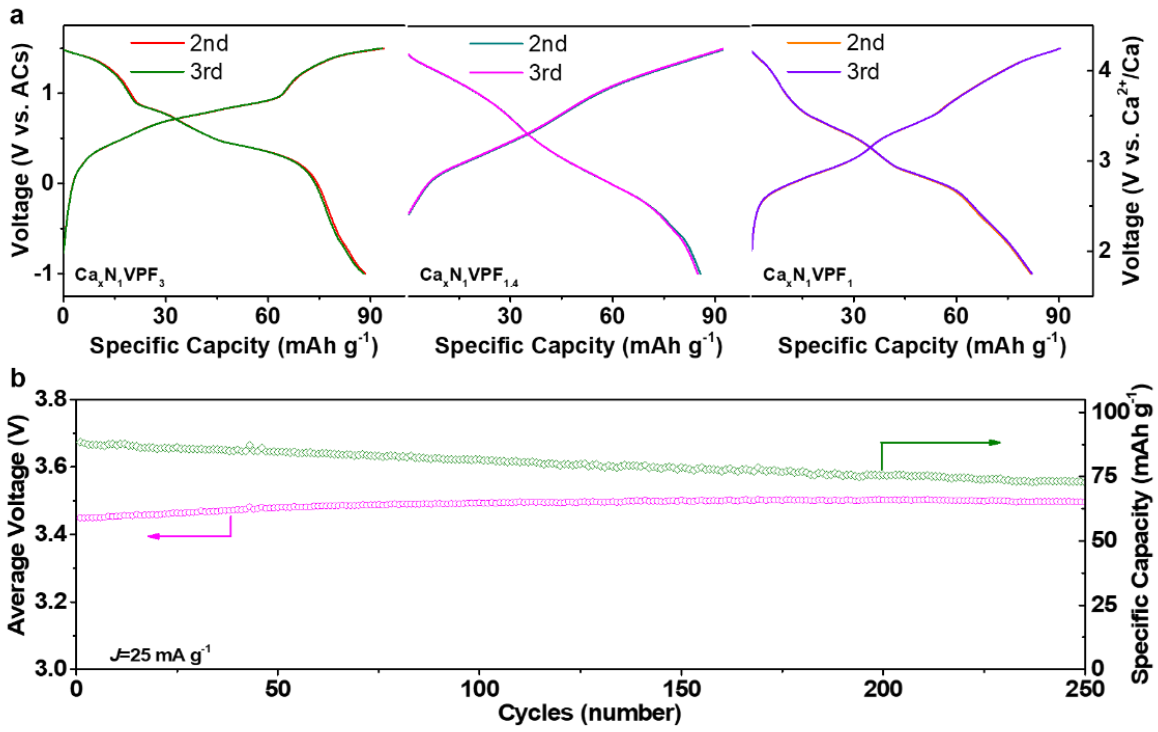

Figure 3. (a) Discharge/charge voltage profiles of N_1VPF_x (x= 1, 1.4, and 3) at 25 mA g^{-1} between -1 and 1.5 V vs. AC, showing similar reversible capacities and distinct average discharge voltages. (b) Average discharge voltage and corresponding specific of N_1VPF_3 cathode during 250 cycles.

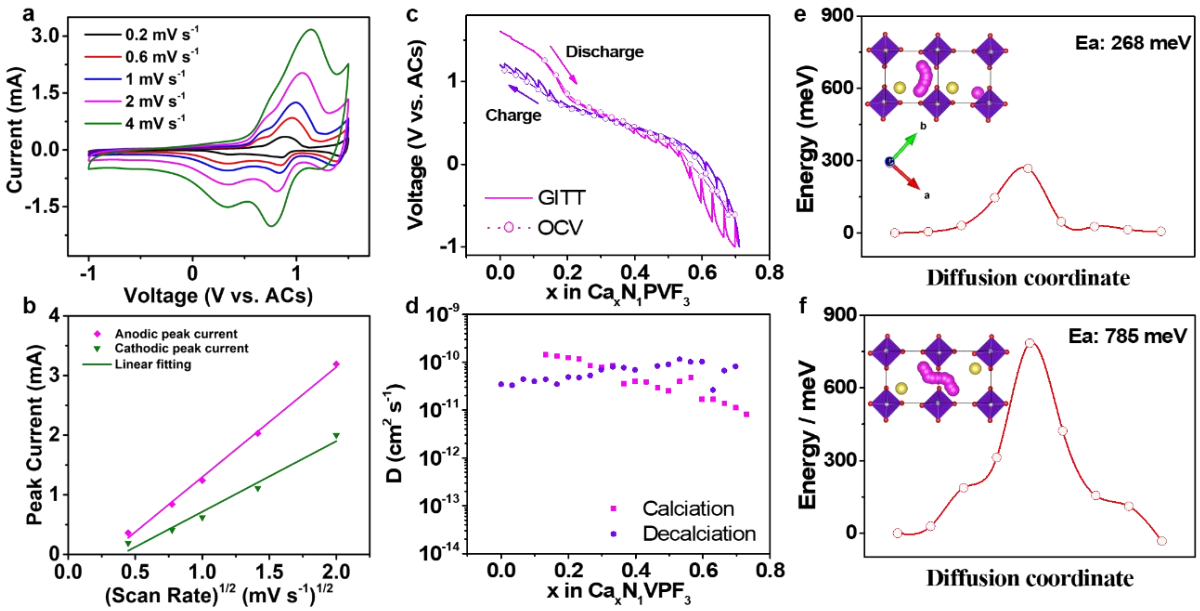

Figure 4. Ca ion migration kinetics in the N_1VPF_3 electrode. (a) CV curves at various scan rates from 0.2 to 4 mV s^{-1}. (b) Linear fits for the anodic and cathodic peak currents versus $v^{1/2}$ derived from CV profiles in (a). (c) Quasi-equilibrium potentials along with the GCD processes of GITT tests and (d) the calculated diffusion coefficiency of Ca^{2+} in N_1VPF_3 cathode during the charge-discharge process. DFT calculated Ca diffusion pathways and diffusion energies for (e) intra-unit and (f) inter-unit paths.

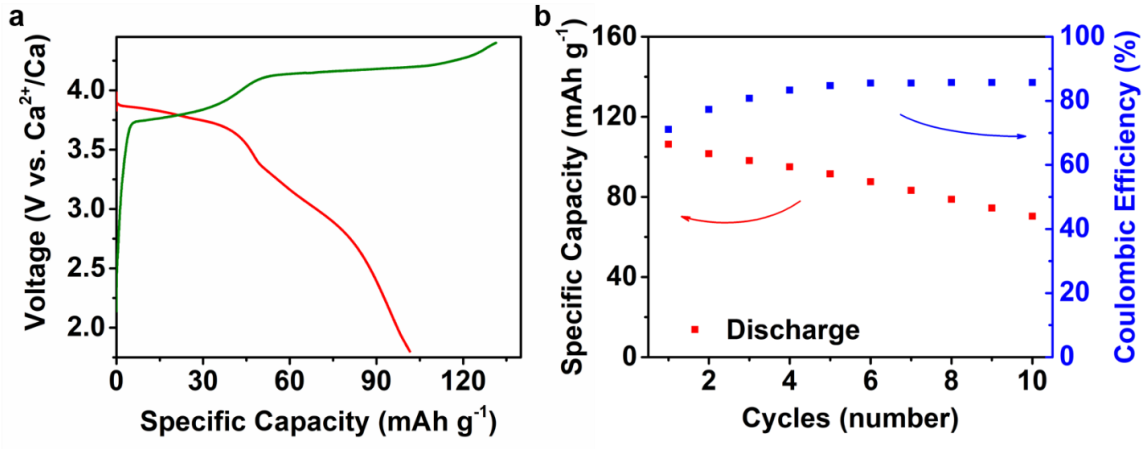

Figure 5. Electrochemical properties of N_1PVF_3//Ca full cells. (a) Charge/discharge voltage curves and (b) the cycling performance at a current density of 10 mA g^{-1} between 1.8-4.4 V vs. Ca^{2+}/Ca.